In-plane thermoelectric properties of graphene/xBN/graphene van der Waals heterostructures

Sylvester W. Makumi^{1,3}, Daniel Bem¹, Nicholas Musila¹, Cameron Foss², Zlatan Aksamija^{2,3}

- ¹ Department of Physics, Kenyatta University, Kenya
- ² Electrical and Computer Engineering, University of Massachusetts Amherst, USA
- ³ Materials Science and Engineering Department, University of Utah, USA

ABSTRACT

2D materials have attracted broad attention from researchers for their unique electronic properties, which may be been further enhanced by combining 2D layers into vertically stacked van der Waals heterostructures. Among the superlative properties of 2D systems, thermoelectric energy (TE) conversion promises to enable targeted energy conversion, localized thermal management, and thermal sensing. However, TE conversion efficiency remains limited by the inherent tradeoff between conductivity and thermopower. In this paper, we use first-principles calculation to study graphene-based van der Waals heterostructures (vdWHs) composed of graphene layers and hexagonal boron nitride (h-BN). We compute the electronic band structures of heterostructured systems using Quantum Espresso and their thermoelectric (TE) properties using BoltzTrap2. Our results have shown that stacking layers of these 2D materials opens a bandgap, increasing it with the number of h-BN interlayers, which significantly improves the power factor (PF). We predict a PF of $\sim 1.0 \times 10^{11}$ W/K².m.s for the vdWHs, nearly double compared to 5×10^{10} W/K².m.s that we obtained for single-layer graphene. This study gives important information on the effect of stacking layers of 2D materials and points toward new avenues to optimize the TE properties of vdWHs.

Key words: Graphene Hexagonal boron nitrade heterostructure thermoelectric Seebeck coefficient

1 INTRODUCTION

Van der Waals heterostructures (vdWHs) are a new class of materials that comprise vertical stacks of different atomically thin, two-dimensional materials. Their properties exhibit new quantum phenomena with potential applications in nano-electronics [1, 2]. For instance, vdWHs are a promising candidate for use in thermoelectric (TE) energy conversion [3–5], energy storage [6], sensors [7], solar cells [8], flexible electronics [2], transistors [1, 2], and optoelectronic devices, such as light-emitting devices, photovoltaics, and photodetectors [1, 2]. TE materials can be used for electricity generation from waste heat via the Seebeck effect or temperature modulation through the Peltier effect.

However, TE performance of currently designed materials is still comparatively low, limiting their application in temperature modulation and power generation. This limitation stems from the fact that the efficiency of TE conversion requires high electrical conductivity and a high Seebeck coefficient simultaneously with low thermal conductivity. These properties are often interdependent and limit our ability to optimize them independently. Therefore, there is an ongoing need for better TE materials.

Low-dimensional materials are potential candidates for designing high-performance TE devices as quantum confinement alters the density of electronic states and shifts the trade-off between conductivity and the Seebeck coefficient by increasing average carrier energy. The potential of these materials was predicted for the first time by Hicks and Dresselhaus in 1993 [9, 10]. Combining layers of different 2D materials provides means of utilizing the signature properties of individual materials and open new pathways for creating heterostructures with unique properties. Many researchers have focused on enhancing the TE performance of materials through reductions in lattice thermal conductivity [11, 12] and improvements in the power factor ($S^2\sigma$) [13-15].

Generally, pure graphene shows a modest TE figure-of-merit, despite its high carrier mobility [16] and power factor [17]. This is mainly attributed to two factors: graphene record-high thermal conductivity [18] and its lack of a bandgap. However, previous studies have shown that the low-energy electronic structure of graphene/h-BN hybrid systems consists of chiral pseudospin doublets [19, 20], which leads to a bandgap opening in graphene sheets [21]. It has been observed that graphene sheets with vertically stacked junctions show increased TE performance [22]. Besides, stacking graphene with other materials, like h-BN, can result in a better TE material [5, 23, 24]. Chen et al., (2014) have experimentally studied the TE performance across graphene/h-BN heterostructure through a gradient of temperature induced between the top and bottom graphene layers and taking measurements corresponding with the open circuit voltage (Δ V) across the heterostructure. A potential difference of 4mV and 39K gradient of temperature (Δ T) were observed, which gives about 99.3 μ VK-1 Seebeck coefficient, a 1.51×10⁻¹⁵W/K² power factor (PF), and a dimensionless figure-ofmerit of 1.05×10⁻⁶ for the heterostructure [25]. Twisted bilayers of graphene have also demonstrated potential for high PF [13]. However, systematic knowledge of the impact of the number of h-BN layers in the vdWHs is lacking.

In this study, we compute the electronic structure and in-plane TE performance of vertically stacked 2D materials composed of atomic layers of graphene and hexagonal boron nitrate (h-BN) using DFT and the Boltzmann transport theory (BTE). We investigate the impact of changing the number of h-BN layers on the electronic and TE performance of the heterostructures and show that the PF of graphene can be doubled by vertically stacking graphene layers with h-BN layers.

2 METHODOLOGY

2.1 Computation details

The first-principles calculation based on DFT as implemented in Quantum Espresso [26–28] has been employed choosing Perdew-Burke-Ernzerhof (PBE) [29] functional, and projector augmented wave (PAW) pseudopotentials. Five materials have been studied; single-layer graphene (G), double-layers graphene (2G), and vdWHs composed of h-BN layers sandwiched between two graphene layers (G/xBN/G, x=1, 2 and 3). The k-grid and cut-off energies used are presented in Table 1, while in Figure 1, we show images of the crystal structures.

Material	k-point grid	ecutwfc(Ry)	ecutrho(Ry)
1 layer G	150x150x1	60	300
2 layer G	152x152x1	34	155
G/BN/G	140x140x1	60	300
G/2BN/G	125x125x1	45	270
G/3BN/G	115x115x1	80	560

Table 1. The k-grid, kinetic energy cutoff (Ry) for wave functions (ecutwfc), and for charge density and potential (ecutrho) used in this study.

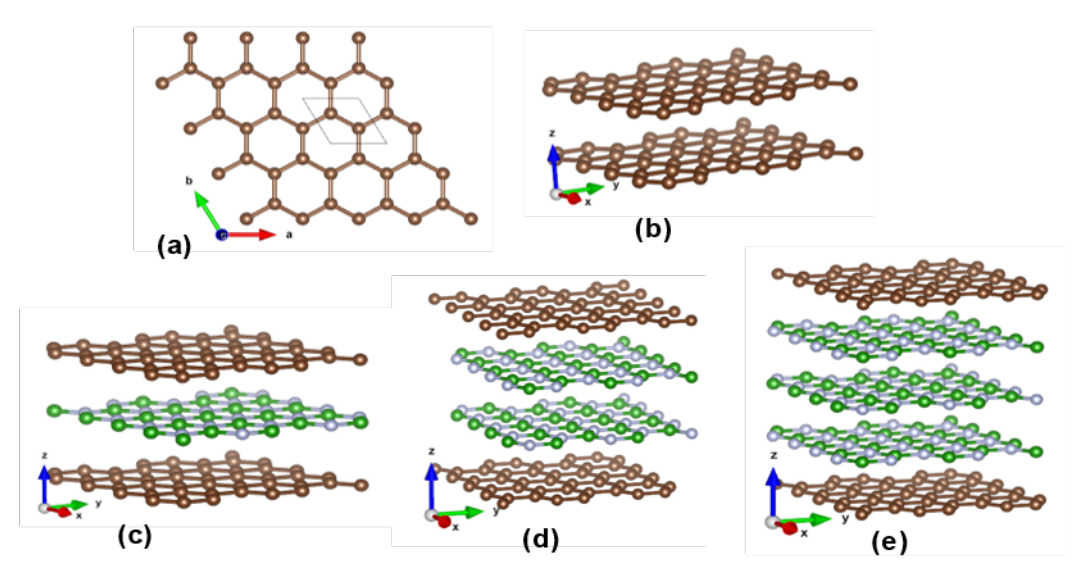


Figure 1. Crystal structures as seen in VESTA software for (a) Image of single-layer graphene showing the primitive cell. (b) double-layer graphene that is AA-stacked in the z-direction. (c), (d), and (e) images of graphene and h-BN heterostructures (G/xBN/G, x=1, 2 and 3) where graphene layers and h-BN layers are AB stacked.

Our samples have been modeled with sufficiently large vacuum space between 13.3 and 17Å in the c-direction. This is to separate them from their images in the c-direction. For the Graphene/BN heterostructures, graphene layers and h-BN layers have been AB stacked where one carbon atom is located in the middle of an h-BN hexagon and one on top of a boron atom. This has been observed to be the most energetically favourable configuration for vdWHs composed of atomic layers of graphene and h-BN [4, 30–34].

To determine TE transport parameters, the semi-classical BTE, as enforced in the BoltzTraP2 code [35], has been applied. The BTE enables us to determine TE transport parameters along two perpendicular principal-axes in the plane of the 2D materials. The TE transport tensors can be defined using the group velocity $v_{\alpha}(i,k)$, which directly employs the band structure data from DFT calculation.

$$v_{\alpha}(i,k) = \frac{\partial \varepsilon(i,k)}{\hbar \partial k_{\alpha}}$$

Here α refers to the α^{th} component of the velocity and "i" to the ith energy band. In the relaxation time approximation (RTA), the electrical conductivity tensor can be expressed as

$$\frac{\sigma_{\alpha\beta}(T,\varepsilon_f)}{\tau} = \frac{1}{\Omega} \int e^2 v_{\alpha}(i,k) v_{\beta}(i,k) \left[-\frac{\partial f_{\varepsilon_f}(T,\varepsilon)}{\partial \varepsilon} \right] d\varepsilon$$
 2

Where Ω is the volume of the unit cell, ε_f is the fermi energy, e is the electronic charge, and τ is the relaxation time of electrons that consists of interactions between electrons and phonons and

impurities in a material's structure. In this study, the value of τ has not been determined; instead, RTA has been adopted.

Here $f_{\varepsilon_f} = \frac{1}{\varepsilon^{-\varepsilon_f}}$ is the Fermi-Dirac distribution function and k_β is the Boltzmann constant.

The thermal conductivity tensor (electronic part) in the RTA is expressed as,

$$\frac{\kappa_{\alpha\beta}^{elec}(T,\varepsilon_f)}{\tau} = \frac{1}{e^2 T \Omega} \int e^2 v_{\alpha}(i,k) v_{\beta}(i,k) \left(\varepsilon - \varepsilon_f\right)^2 \left[-\frac{\partial f_{\varepsilon_f}(T,\varepsilon)}{\partial \varepsilon} \right] d\varepsilon , \qquad 3$$

and the Seebeck coefficient tensor can be written as,

$$S_{\alpha\beta}(T,\varepsilon_f) = \frac{1}{eT} \frac{\int \nu_{\alpha}(i,k)\nu_{\beta}(i,k) \left(\varepsilon - \varepsilon_f\right) \left[\frac{-\partial f_{\varepsilon_f}(T,\varepsilon)}{\partial \varepsilon}\right] d\varepsilon}{\int \nu_{\alpha}(i,k)\nu_{\beta}(i,k) \left[\frac{-\partial f_{\varepsilon_f}(T,\varepsilon)}{\partial \varepsilon}\right] d\varepsilon}.$$

The PF is the product of the square of the Seebeck coefficient and electrical conductivity and can be written as,

$$PF = S_{\alpha\beta}^{2}(T, \varepsilon_{f})\sigma_{\alpha\beta}(T, \varepsilon_{f}).$$
 5

Using the BoltzTraP2 program, we have solved equations 2-5 to give as output the S, σ , k^{elec} , and PF transport tensors at different energy levels, temperatures, and charge carrier concentrations.

3 RESULTS AND DISCUSSION

3.1 Band structure and DOS

The calculated band structures and DOS for the five materials are presented in Figures 2 and 3. We show that the valence band maximum (VBM) and the conduction band minimum (CBM) occur at the Dirac points K and K' in the k-space. Single-layer graphene is a zero band-gap material with linear energy dispersion.

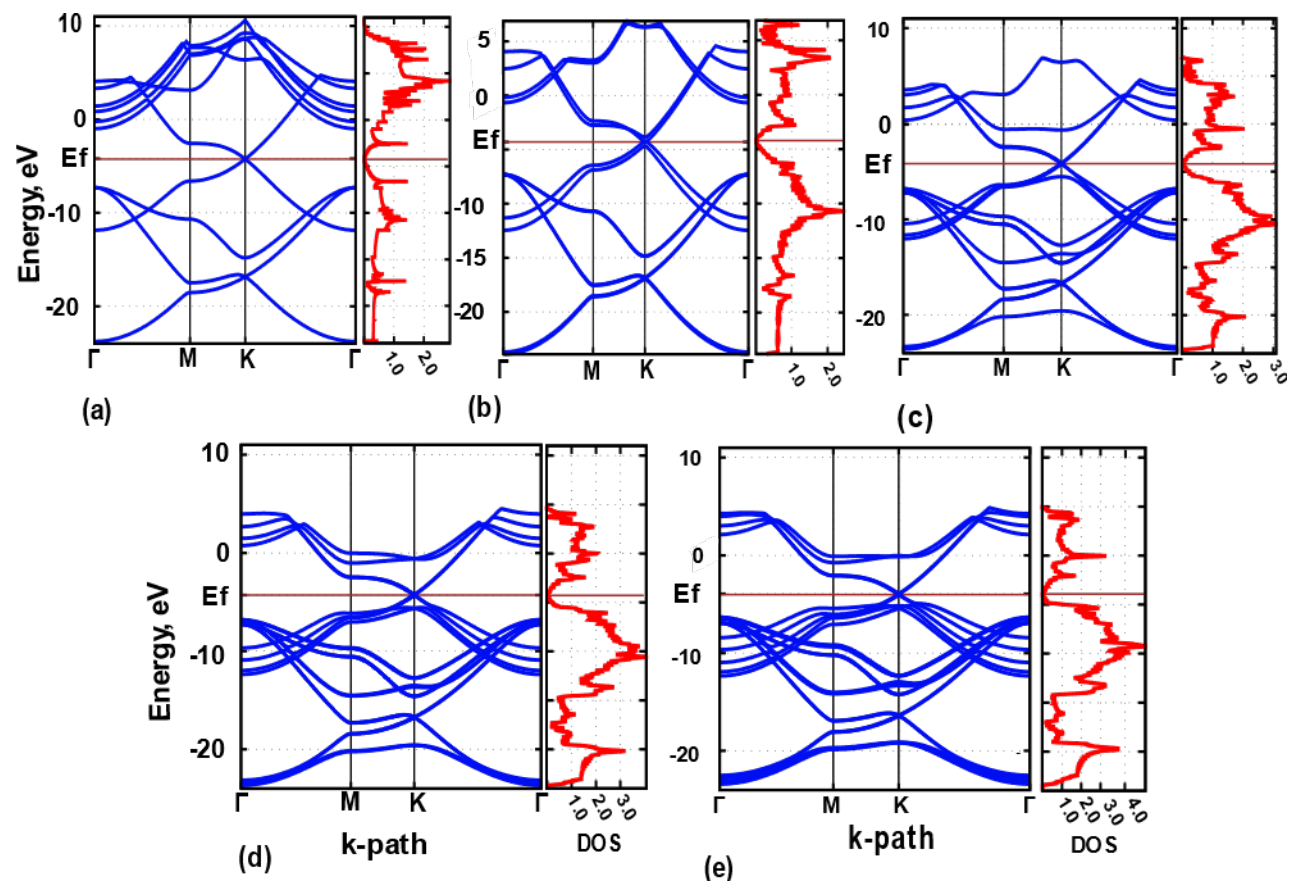


Figure 2. Electronic band-structure along the high symmetry path and DOS for (a) band-structure and DOS of single-layer graphene, (b) band-structure and DOS of double-layer graphene, (c) band-structure and DOS of G/BN/G, (d) band-structure and DOS of G/2BN/G (e) band-structure and DOS of G/3BN/G. For all the materials, the valence band maximum (VBM) and the conduction band minimum (CBM) occur at the Dirac points K and K' in the k-space.

In moving from single to two-layer graphene, a band gap does not open yet, but the bands become parabolic near the Fermi level. Adding one layer of h-BN (forming G/BN/G) also doesn't open a band gap. However, the addition of more h-BN layers opens a gap that increases with the number of h-BN layers, which is consistent with previous studies [21, 33]. This has been attributed to the pseudospin interactions [19-21]. We observe a band-gap of 0.089eV and 0.131eV for G/2BN/G and G/3BN/G, respectively.

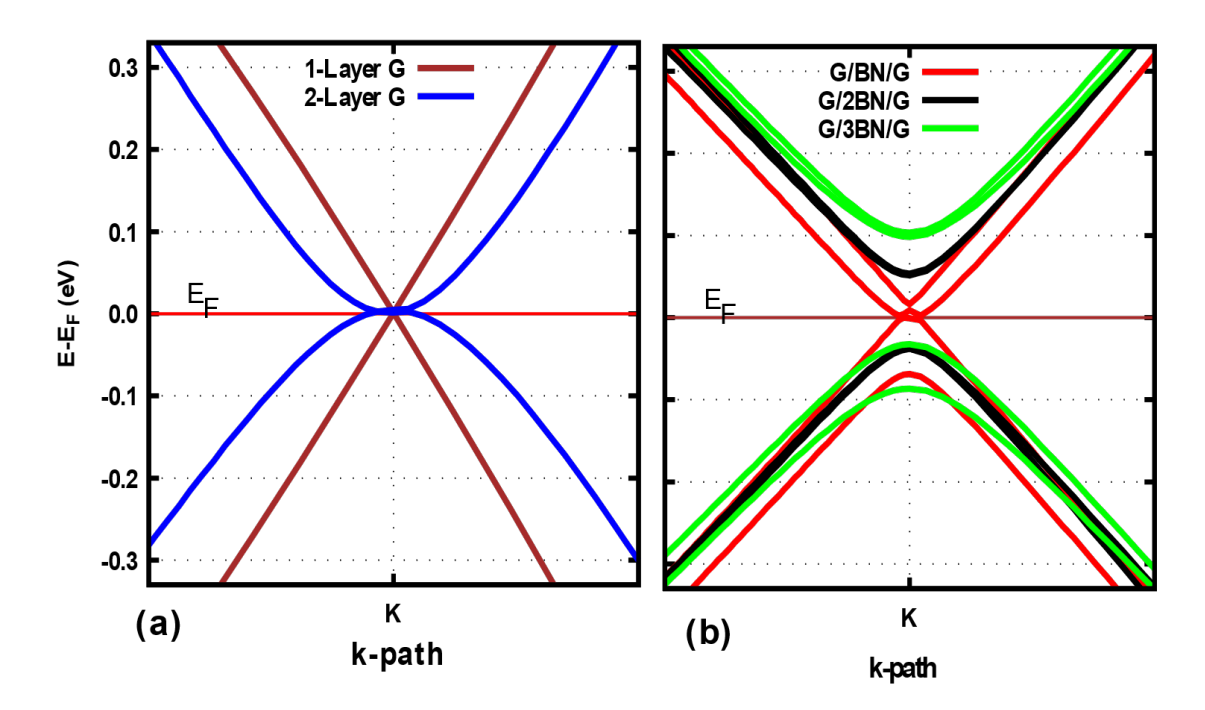


Figure 3. The band structures near the fermi level (a) the band structure of single-layer graphene and two-layer graphene. Single-layer graphene has a linear structure, while the band structure of double-layer graphene is parabolic near the Fermi level. (b) the band structure of G/BN/G with no band-gap, G/2BN/G with a band-gap of 0.089eV, and G/3BN/G with a band-gap of 0.131eV showing increasing band-gap with an increase in h-BN layers.

The velocity of carriers which is determined from the slope of the electronic structure, decreases with the addition of h-BN layers, thus, reducing the electrical conductivity of the material. Besides, a sharp feature is created in the DOS curve, which leads to an increase in the Seebeck coefficient.

3.2 Thermoelectric Properties

3.2.1 Seebeck coefficient

In this study, the Seebeck coefficient has been presented as a function of energy and absolute temperature T. In Figure 4, S at 300K has been plotted as a function of energy. Since h-BN has a large band-gap relative to graphene, the electric conduction of graphene/h-BN heterostructure is mainly determined by the two graphene sheets on the heterostructure film. Consequently, the observed S for the vdWHs has features that are very similar to that of the graphene sheet.

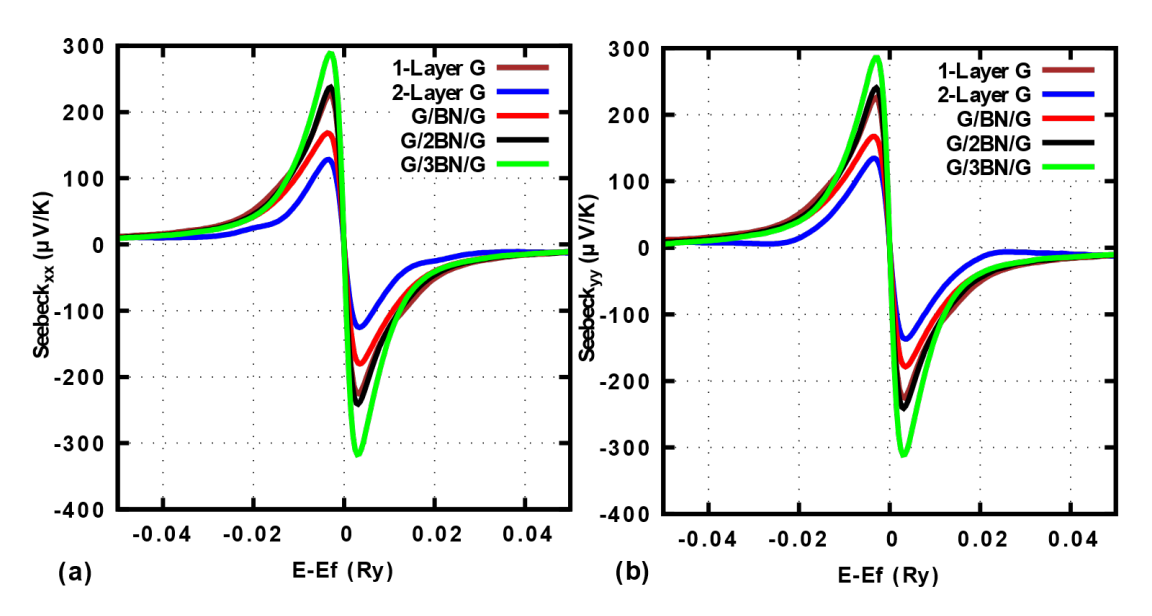


Figure 4. Seebeck coefficient at 300K (a) in the x-direction (zigzag direction) and (b) in the y-direction (armchair direction). The peak values of the Seebeck coefficient in the positive and negative values of E-EF and in the x and y are within the same values.

In Table 2, the peak values of S and PF for all the materials are presented. Peak values of the Seebeck coefficient for the n-type (negative) and p-type (positive) are about the same values. Our values for the Seebeck coefficient are within the range of previously reported values. D'Souza and Mukherjee have predicted (using BoltzTraP2) a Seebeck coefficient of $180\text{-}250\mu\text{V/K}$ and $100\text{-}150~\mu\text{V/K}$ for single and bi-layer graphene, respectively [5]. We observe PF of $\sim 1x10^{11}~(\text{W/K}^2\text{.m.s})$ for the vdWHs, which is double that of single-layer graphene of $5x10^{10}~(\text{W/K}^2\text{.m.s})$.

MATERIAL	Sxx (μV/K)	Syy (μV/K)	PF/Tau_{xx} *10 ¹¹ (W/K ² .m.s)	PF/Tau_{yy} *10 ¹¹ (W/K ² .m.s)
1 layer G	226	226	0.47236	0.53244
2 layer G	125	137	1.17484	2.092930
G/BN/G	180	179	0.89278	1.079900
G/2BN/G	241	241	0.74631	0.909622
G/3BN/G	317	311	0.88904	1.100140

Table 2: Peak values of S and PF at room temperature for all our materials. It is observed that the PF values of graphene/h-BN vdWHs are 50% greater compared to single-layer graphene.

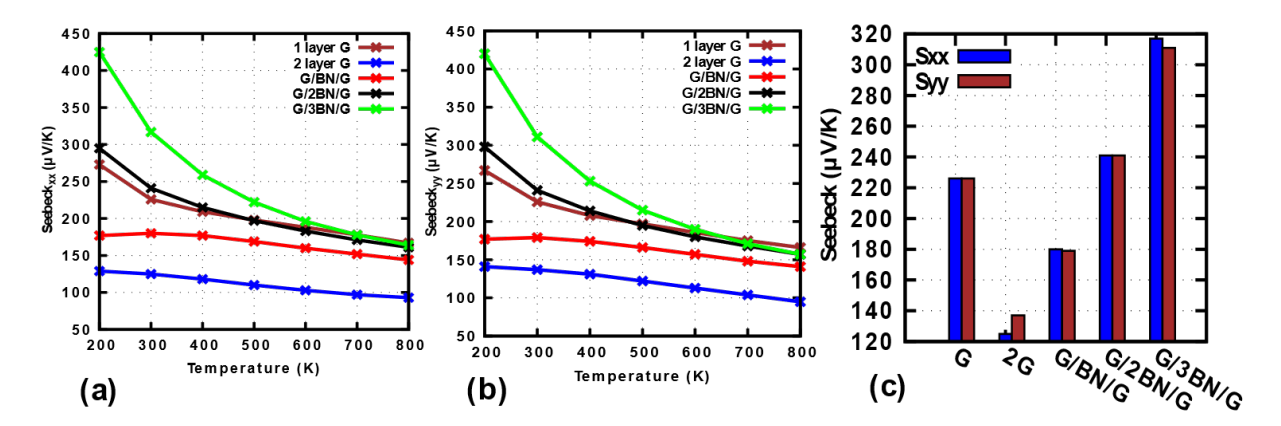


Figure 5. Seebeck Coefficient as a function of temperature in (a) x-direction (zigzag direction) and (b) y-direction (armchair direction)(c) Seebeck coefficients for different samples at 300K. Seebeck decreases with increasing temperature but increases with increasing number of h-BN layers.

As shown in Figure 5, the in-plane Seebeck coefficient in the x- and y-directions decreases with an increase in temperature. We have observed that S increases with increasing number of h-BN layers. This can be related to the increasing bandgap with the number of h-BN layers, which creates a sharper feature in the DOS, leading to an increase in S. We have also observed that single-layer graphene has a higher S than bi-layer graphene which is in good agreement with previous studies [4, 5].

We observe that the temperature-dependence of the Seebeck coefficient is more pronounced in vdWHs with more h-BN layers, with the system consisting of three layers of h-BN being the most affected. The Seebeck coefficient for G/BN/G, G/2BN/G, and G/3BN/G decrease by 19%, 46%, and 62% when the temperature is increased from 200 to 800 K. This is attributed to the electronic structure of the materials at the K point; the temperature dependence is stronger when there is a band-gap and a sharp feature of the DOS which ensures a high increase rate of carriers with increasing temperature.

3.2.2 Electrical conductivity

The electrical conductivity (σ) as a function of energy, which has been determined using Boltzmann transport theory from equation 2, is presented in Figure 6(a & b). Generally, for semiconductors, as we move from the intrinsic Fermi energy, we have increasing DOS hence increasing electrical conductivity. This has been clearly observed in this study, as shown in Figure 6. We have extracted data for σ/τ at E-Ef=0.0025 Ry (0.03401 eV), the energy around which we have the peak values of the Seebeck coefficient, and shown it in Figure 6 over a temperature range from 100 to 800K. Increasing temperature leads to more thermally excited electrons hence increasing the electrical conductivity of the materials. It has been observed that the electrical conductivity of our vdWHs decreases with

increasing h-BN layers. The electronic thermal conductivity shows the same behavior as the electrical conductivity, as expected.

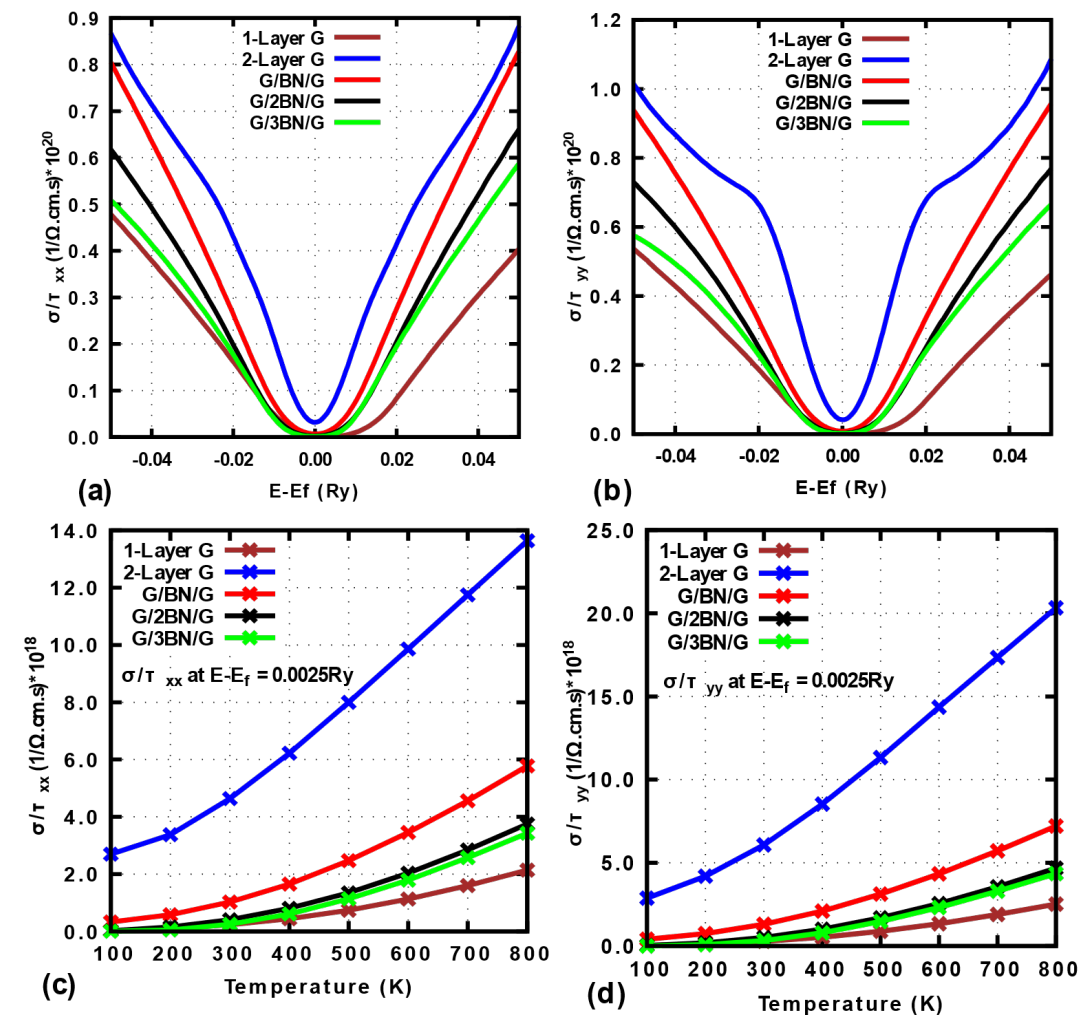


Figure 6. The electrical conductivity in the (a) x- direction zigzag direction) and (b) y- directions (armchair direction) at 300K. The electrical conductivity in the (c) x- and (d) y- directions as a function of temperature. Electrical conductivity decreased with an increasing number of h-BN layers and temperature.

3.2.3 Power factor (PF)

We have observed a PF of $1.1x10^{11}$ W/K².m.s for G/3BN/G at room temperature. From Figure 7, it can be observed that the PF increases with temperature. Graphene/h-BN heterostructure shows a higher PF than single-layer graphene. However, PF for double-layer graphene is the highest, which can be attributed to its high electrical conductivity, as seen in Figure 6. Besides, for heterostructures with h-BN, increases in the Seebeck are cancelled by decreases in the electrical conductivity; hence there is little impact on the PF when adding h-BN layers.

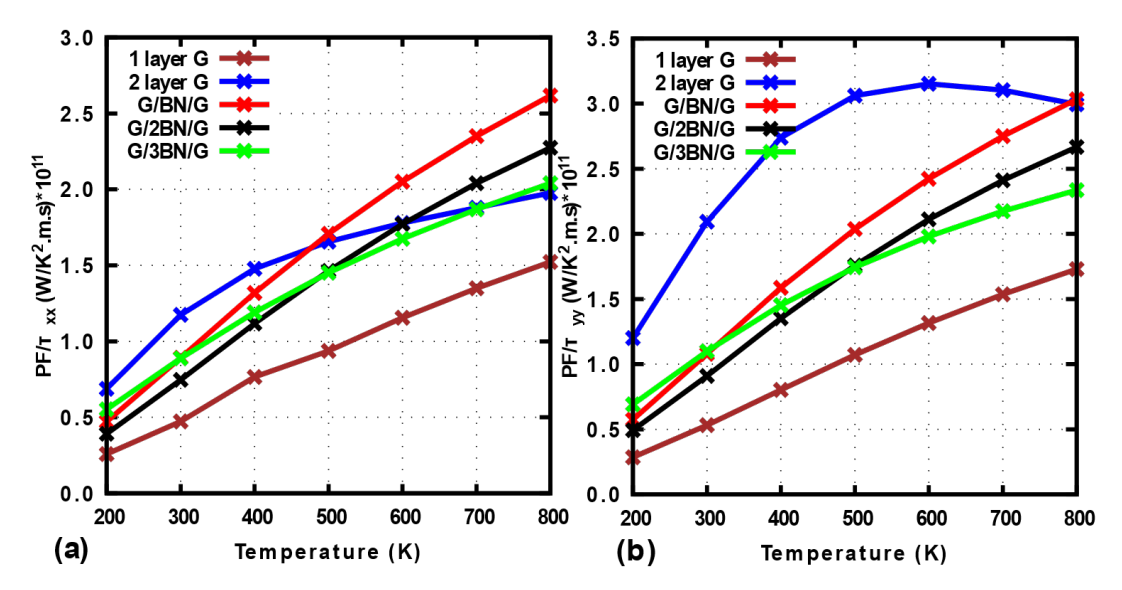


Figure 7. The PF as a function of temperature in the (a) x-direction (zigzag direction) and (b) y-directions (armchair direction). For all samples, the PF increases with increasing temperature. Graphene/h-BN shows higher PF compared to single-layer graphene.

The thermal conductivity of single-layer h-BN is $\sim 751\pm 340$ W/m.K near room temperature [36], significantly lower than that of graphene (about 3400 W/m.K [37]); therefore, adding h-BN layers will lower the thermal conductivity of the combined system relative to that of graphene. In addition, interlayer interactions between phonons in graphene with phonons in h-BN can lower thermal conductivity, analogous to how adding graphene layers to form graphite lower thermal conductivity to about 2000 W/m.K in graphite [38, 39]. Besides, it has been demonstrated that increasing the number of h-BN layers lowers the material's thermal conductivity [36]. This decrease in thermal conductivity is expected to improve the ZT value of the heterostructure.

It is worth noting that as the number of h-BN layers increases, eventually, the h-BN stack becomes too thick for the graphene layers to interact. We expect a limit at about ten layers of h-BN [40], beyond which h-BN will show bulk characteristics, and adding more h-BN layers will deteriorate the thermoelectric properties of the heterostructure. We can think of this limit as two graphene monolayers separated by bulk h-BN so that each graphene layer act akin to a monolayer on h-BN substrate. Besides, thick h-BN will have a large band-gap and act as an insulator. Therefore, the Seebeck coefficient of the vdWHs will be high (since the Fermi level is in the band-gap); however, electrical conductivity will be minuscule, leading to a low PF and hence a tiny ZT value.

4 CONCLUSION

In conclusion, this paper has discussed the TE properties of G/xBN/G vdWHs and compared them with that of isolated single- and double-layer graphene. We observe that h-BN layers sandwiched between graphene layers lower electrical conductivity and electronic thermal conductivity but increase the Seebeck coefficient and PF. The Seebeck coefficient of double-layer graphene increase by a factor of 2.5 when three layers of h-BN are sandwiched between them. We find that adding three layers of h-BN doubles the PF of the graphene sheet. A bandgap is introduced that increases with the number of h-BN layers. It has been observed that the impact of change in temperature on the Seebeck coefficient (S) of samples increases with the number of h-BN layers, with the sample composed of three h-BN layers being the most affected where S decreases by 62% for a temperature change from 200K to 800K. This work shows that band structure modifications arising from vertically stacking layers of 2D materials can be used to achieve increases in TE performance not seen in constituent 2D materials.

ACKNOWLEDGEMENT

We acknowledge support from the National Science Foundation Grant #1902352 and the University of Massachusetts Amherst (UMass); all calculations in this study were carried out using the UMass GHPCC computer cluster.

REFERENCES

- [1] S.-J. Liang, B. Cheng, X. Cui, and F. Miao, "Van der Waals Heterostructures for High-Performance Device Applications: Challenges and Opportunities," *Adv. Mater.*, vol. 32, no. 27, p. 1903800, Jul. 2020, doi: 10.1002/ADMA.201903800.
- [2] Y. Liu, N. O. Weiss, X. X. Duan, H. C. Cheng, Y. Huang, and X. X. Duan, "Van der Waals heterostructures and devices," *Nat. Rev. Mater.*, vol. 1, no. 9, pp. 1–17, Jul. 2016, doi: 10.1038/natreymats.2016.42.
- [3] M. Markov and M. Zebarjadi, "Thermoelectric transport in graphene and 2D layered materials," *Nanoscale Microscale Thermophys. Eng.*, vol. 23, no. 2, pp. 117–127, 2018, doi: 10.1080/15567265.2018.1520762.
- [4] J. Wang *et al.*, "The thermal and thermoelectric properties of in-plane C-BN hybrid structures and graphene/h-BN van der Waals heterostructures," *Mater. Today Phys.*, vol. 5, pp. 29–57, Jun. 2018, doi: 10.1016/j.mtphys.2018.05.006.
- [5] R. D'souza and S. Mukherjee, "First principles calculation of thermoelectric parameters of Monolayer- and Bilayer-Graphene and Heterostructures of Graphene and h-BN," *J. Phys. Conf. Ser.*, vol. 759, no. 1, p. 012040, Oct. 2016, doi: 10.1088/1742-6596/759/1/012040.
- [6] S. Wang, S. Zhao, X. Guo, and G. Wang, "2D Material-Based Heterostructures for Rechargeable Batteries," *Adv. Energy Mater.*, vol. 12, no. 4, p. 2100864, Jan. 2022, doi: 10.1002/AENM.202100864.
- [7] Z. L. Lei and B. Guo, "2D Material-Based Optical Biosensor: Status and Prospect," *Adv. Sci.*, vol. 9, no. 4, p. 2102924, Feb. 2022, doi: 10.1002/ADVS.202102924.
- [8] M. J. Molaei, M. Younas, and M. Rezakazemi, "Van der Waals heterostructures in ultrathin 2D solar cells: State-of-the-art review," *Mater. Sci. Eng. B*, vol. 285, p. 115936, Nov. 2022, doi: 10.1016/J.MSEB.2022.115936.
- [9] L. D. Hicks and M. S. Dresselhaus, "Thermoelectric figure of merit of a one-dimensional conductor," *Phys. Rev. B*, vol. 47, no. 24, pp. 16631–16634, 1993, doi: 10.1103/PhysRevB.47.16631.
- [10] L. D. Hicks and M. S. Dresselhaus, "Effect of quantum-well structures on the thermoelectric figure of merit," *Phys. Rev. B*, vol. 47, no. 19, pp. 12727–12731, 1993, doi: 10.1103/PhysRevB.47.12727.
- [11] N. Kumar, P. K. Sachdeva, R. Gupta, and C. Bera, "Theoretical Design of Highly Efficient 2D Thermoelectric Device Based on Janus MoSSe and Graphene Heterostructure," *ACS Appl. Energy Mater.*, vol. 5, no. 8, pp. 9581–9586, Aug. 2022, doi: 10.1021/ACSAEM.2C01204/SUPPL FILE/AE2C01204 SI 001.PDF.
- [12] J. Gu, L. Huang, and S. Liu, "Ultralow lattice thermal conductivity and high thermoelectric performance of monolayer KCuTe: A first principles study," *RSC Adv.*, vol. 9, no. 62, pp. 36301–36307, 2019, doi: 10.1039/c9ra07828b.

- [13] A. Kommini and Z. Aksamija, "Very high thermoelectric power factor near magic angle in twisted bilayer graphene," *2D Mater.*, vol. 8, no. 4, p. 045022, Oct. 2021, doi: 10.1088/2053-1583/AC161D.
- [14] A. K. Majee, A. Kommini, and Z. Aksamija, "Electronic Transport and Thermopower in 2D and 3D Heterostructures—A Theory Perspective," *Ann. Phys.*, vol. 531, no. 9, p. 1800510, Sep. 2019, doi: 10.1002/andp.201800510.
- [15] J. P. Heremans, B. Wiendlocha, and A. M. Chamoire, "Resonant levels in bulk thermoelectric semiconductors," *Energy Environ. Sci.*, vol. 5, no. 2, pp. 5510–5530, Jan. 2012, doi: 10.1039/C1EE02612G.
- [16] K. I. Bolotin *et al.*, "Ultrahigh electron mobility in suspended graphene," *Solid State Commun.*, vol. 146, no. 9–10, pp. 351–355, Jun. 2008, doi: 10.1016/j.ssc.2008.02.024.
- [17] J. Duan *et al.*, "High thermoelectric power factor in graphene/hBN devices," *Proc. Natl. Acad. Sci. U. S. A.*, vol. 113, no. 50, pp. 14272–14276, Dec. 2016, doi: https://doi.org/10.1073/pnas.1615913113.
- [18] A. A. Balandin *et al.*, "Superior Thermal Conductivity of Single-Layer Graphene," *Nano Lett.*, vol. 8, pp. 902–907, 2008.
- [19] I. Zasada, P. Maślanka, A. Molenda, and K. Łuczak, "H-BN-layer-induced chiral decomposition in the electronic properties of multilayer graphene," *J. Phys. Condens. Matter*, vol. 30, no. 5, 2018, doi: 10.1088/1361-648X/aa9fd9.
- [20] A. Molenda, I. Zasada, and P. Maślanka, "Chiral properties of graphene h-BN hybrid systems," *Phys. E Low-Dimensional Syst. Nanostructures*, vol. 107, no. November 2018, pp. 160–169, 2019, doi: 10.1016/j.physe.2018.11.033.
- [21] J. Yan *et al.*, "Graphene homojunction: Closed-edge bilayer graphene by pseudospin interaction," *Nanoscale*, vol. 8, no. 17, pp. 9102–9106, 2016, doi: 10.1039/c5nr08083e.
- [22] V. H. Nguyen, M. C. Nguyen, H.-V. Nguyen, J. Saint-Martin, and P. Dollfus, "Enhanced thermoelectric figure of merit in vertical graphene junctions," *Appl. Phys. Lett.*, vol. 105, no. 13, pp. 1–5, Sep. 2014, doi: 10.1063/1.4896915.
- [23] V. T. Tran, J. Saint-Martin, and P. Dollfus, "High thermoelectric performance in graphene nanoribbons by graphene/BN interface engineering," *Nanotechnology*, vol. 26, no. 49, pp. 1–17, May 2015, doi: 10.1088/0957-4484/26/49/495202.
- [24] X.-M. M. Wang and S.-S. S. Lu, "First-Principles Study of the Transport Properties of Graphene-Hexagonal Boron Nitride Superlattice," *J. Nanosci. Nanotechnol.*, vol. 15, no. 4, pp. 3025–3028, Apr. 2015, doi: 10.1166/jnn.2015.9636.
- [25] C.-C. C. Chen, Z. Li, L. Shi, and S. B. Cronin, "Thermoelectric transport across graphene/hexagonal boron nitride/graphene heterostructures," *Nano Res.*, vol. 8, no. 2, pp. 666–672, Feb. 2014, doi: 10.1007/s12274-014-0550-8.

- [26] P. Giannozzi *et al.*, "QUANTUM ESPRESSO: a modular and open-source software project for quantum simulations of materials," *J. Phys. Condens. Matter*, vol. 21, no. 39, p. 395502, Sep. 2009, doi: 10.1088/0953-8984/21/39/395502.
- [27] P. Giannozzi *et al.*, "Quantum ESPRESSO toward the exascale," *J. Chem. Phys.*, vol. 152, no. 15, p. 154105, Apr. 2020, doi: 10.1063/5.0005082.
- [28] P. Giannozzi *et al.*, "Advanced capabilities for materials modelling with Quantum ES-PRESSO," *J. Phys. Condens. Matter*, vol. 29, no. 46, p. 465901, Oct. 2017, doi: 10.1088/1361-648X/AA8F79.
- [29] J. P. Perdew, K. Burke, and M. Ernzerhof, "Generalized Gradient Approximation Made Simple," *Phys. Rev. Lett.*, vol. 77, no. 18, p. 3865, Oct. 1996, doi: 10.1103/PhysRevLett.77.3865.
- [30] Y. Sakai, T. Koretsune, and S. Saito, "Electronic structure and stability of layered superlattice composed of graphene and boron nitride monolayer," *Phys. Rev. B Condens. Matter Mater. Phys.*, vol. 83, no. 20, pp. 1–8, 2011, doi: 10.1103/PhysRevB.83.205434.
- [31] Q. Gao *et al.*, "Structural Determination of a Graphite/Hexagonal Boron Nitride Superlattice Observed in the Experiment," *Inorg. Chem.*, vol. 60, no. 4, pp. 2598–2603, 2021, doi: 10.1021/acs.inorgchem.0c03479.
- [32] G. J. Slotman, G. A. De Wijs, A. Fasolino, and M. I. Katsnelson, "Phonons and electron-phonon coupling in graphene-h-BN heterostructures," *Ann. Phys.*, vol. 526, no. 9–10, pp. 381–386, 2014, doi: 10.1002/andp.201400155.
- [33] G. Giovannetti, P. A. Khomyakov, G. Brocks, P. J. Kelly, and J. Van Den Brink, "Substrate-induced band gap in graphene on hexagonal boron nitride: Ab initio density functional calculations," *Phys. Rev. B Condens. Matter Mater. Phys.*, vol. 76, no. 7, p. 073103, Aug. 2007, doi: 10.1103/PhysRevB.76.073103.
- [34] B. Sachs, T. O. Wehling, M. I. Katsnelson, and A. I. Lichtenstein, "Adhesion and electronic structure of graphene on hexagonal boron nitride substrates," *Phys. Rev. B Condens. Matter Mater. Phys.*, vol. 84, no. 19, p. 195414, Nov. 2011, doi: 10.1103/PhysRevB.84.195414.
- [35] G. K. H. Madsen, J. Carrete, and M. J. Verstraete, "BoltzTraP2, a program for interpolating band structures and calculating semi-classical transport coefficients," *Comput. Phys. Commun.*, vol. 231, pp. 140–145, 2018, doi: 10.1016/j.cpc.2018.05.010.
- [36] Q. Cai *et al.*, "High thermal conductivity of high-quality monolayer boron nitride and its thermal expansion," *Sci. Adv.*, vol. 5, no. 6, pp. 1–9, 2019, doi: 10.1126/sciadv.aav0129.
- [37] D. L. Nika, E. P. Pokatilov, A. S. Askerov, and A. A. Balandin, "Phonon thermal conduction in graphene: Role of Umklapp and edge roughness scattering," *Phys. Rev. B Condens. Matter Mater. Phys.*, vol. 79, no. 15, 2009, doi: 10.1103/PhysRevB.79.155413.
- [38] C. Wang, J. Guo, L. Dong, A. Aiyiti, X. Xu, and B. Li, "Superior thermal conductivity in suspended bilayer hexagonal boron nitride," Sci. Rep., vol. 6, 2016, doi: 10.1038/srep25334.

- [39] L. Lindsay, D. A. Broido, and N. Mingo, "Flexural phonons and thermal transport in multi-layer graphene and graphite," *Phys. Rev. B Condens. Matter Mater. Phys.*, vol. 83, no. 23, pp. 1–5, 2011, doi: 10.1103/PhysRevB.83.235428.
- [40] S. Roy *et al.*, "Structure, Properties and Applications of Two-Dimensional Hexagonal Boron Nitride," *Adv. Mater.*, vol. 33, no. 44, pp. 1–48, 2021, doi: 10.1002/adma.202101589.